Composites: Part A 166 (2023) 107395

Contents lists available at ScienceDirect

Composites Part A

journal homepage: www.elsevier.com/locate/compositesa

Investigation of fracture process zone development in quasi-isotropic carbon/epoxy laminates using *in situ* and *ex situ* X-ray Computed Tomography

Xiaodong Xu [a,b,*], Shin-ichi Takeda [c], Michael R. Wisnom [b]

[a] University of the West of England, Coldharbour Lane, Bristol BS16 1QY, United Kingdom
[b] Bristol Composites Institute, University of Bristol, Queens Building, University Walk, Bristol BS8 1TR, United Kingdom
[c] Aviation Technology Directorate, Japan Aerospace Exploration Agency, 6-13-1 Osawa, Mitaka-shi, Tokyo 181-0015, Japan

ARTICLE INFO

Keywords:
A. Laminates
B. Fracture
B. Fracture toughness
D. CT analysis

ABSTRACT

Trans-laminar fracture toughness is an important property of laminated composites and examining the fracture process zone at the tip of a crack is key to understanding it. To date, little research has been done on in-depth examination of the early fracture process zone development in quasi-isotropic laminates. In this work, detailed *in situ* X-ray Computed Tomography (CT) analyses enabled continuous examination under loading and better understanding of the entire fracture process zone development. *Ex situ* CT scanning of an additional hot temperature wet conditioned specimen with dye penetrant was also employed as a comparison to explain the significance of 0° splitting to *trans*-laminar fracture.

1. Introduction

Despite the extensive research on failure of advanced composites, it is still an urgent issue to better understand their *trans*-laminar fracture. To determine the *trans*-laminar fracture toughness, the examination of fracture process zone is key. This is because there is not a clear crack at the notch tip of a composite laminate, but a complex zone of sub-critical damage and fibre breakage, making it difficult to define the crack length. Different researchers have developed a wide range of *in situ* measurement methods. For example, Pinho et al. [1] used compact tension specimens and an *in situ* optical crack measurements. Zobeiry et al. [2] adopted Over-height Compact Tension (OCT) specimens and Digital Image Correlation (DIC) for measuring the size of the fracture process zone. Catalanotti et al. [3] and Bergan et al. [4] conducted compact tension tests and used DIC to characterise fracture properties. These *in situ* measurements are limited to the specimen surface, making it hard to observe the evolution of internal damage. Other methods do not rely on direct measurements, but some assumptions are made. Catalanotti et al. [5] combined double-edge-notched tensile test results with a size effect law to determine R-curves, deriving the size of the fracture process zone indirectly. Maimí et al. [6] referred to the available OCT results from the literature and applied an equivalent crack length as a result of the experimental normalized compliance.

In contrast, X-ray Computed Tomography (CT) scanning can yield accurate and objective results when assessing the detailed internal damage states. X-ray CT scanning of polymer composites has been reviewed by Garcea et al. [7]. *Ex situ* CT scanning has already been implemented in the studies of *trans*-laminar fracture propagation [8,9]. More recently Rev et al. [10] examined *trans*-laminar fracture in both multi-directional and woven carbon/epoxy laminates, demonstrating the effects of material architecture on fracture propagation. These *ex situ* CT scans require the tests to be interrupted and the specimen to be removed from the test machine. *In situ* CT scanning is an attractive alternative [11], since it enables continuous damage examination under loading. Sun et al. [12] successfully conducted *in situ* CT scanning and used it to characterise *trans*-laminar fracture toughness for laminated composites. They concluded that ASTM E1922 standard [13] and carefully measured fracture process zones can be used to derive initial R-curves. However, they did not examine fracture initiation or fracture process zone development due to limited experimental data.

Many studies have emphasized *trans*-laminar fracture propagation [2,8–10], also referred to as self-similar or steady-state crack propagation. In contrast, few studies have been reported about early fracture process zone development before fracture propagation i.e. before all the plies are broken, including the ±45° as defined by Xu et al. [8]. The closest is the study of damage zones in scaled centre-notched tensile

* Corresponding author.
E-mail address: xiaodong.xu@uwe.ac.uk (X. Xu).

https://doi.org/10.1016/j.compositesa.2022.107395
Received 28 September 2022; Received in revised form 22 November 2022; Accepted 21 December 2022
Available online 24 December 2022

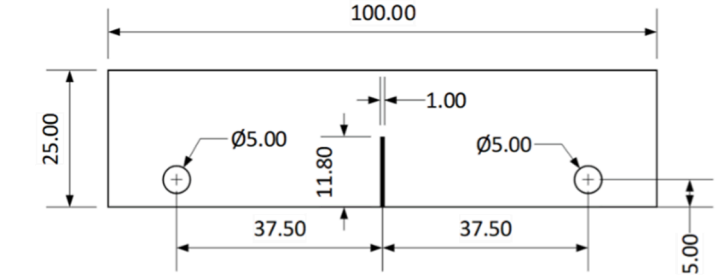

a) *In situ* CT scan specimen geometry and dimensions (mm)

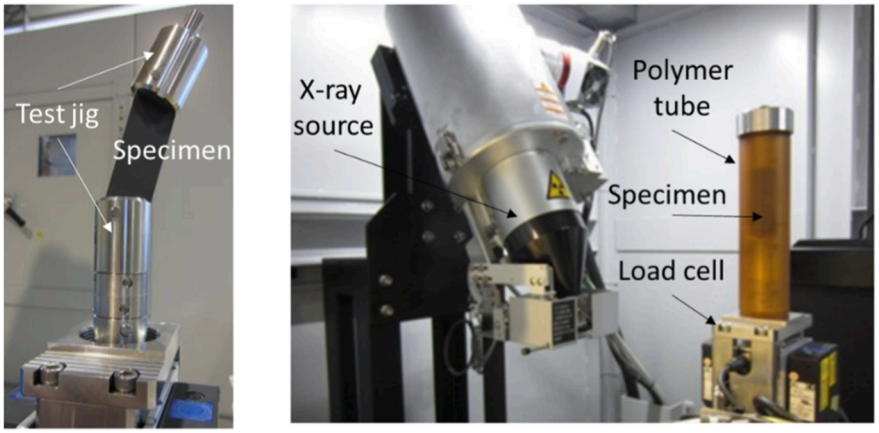

b) Jig assembly before testing c) Test jig set-up for scanning

Fig. 1. *In situ* CT scan specimen and test set-up at JAXA. (For interpretation of the references to colour in this figure legend, the reader is referred to the web version of this article.)

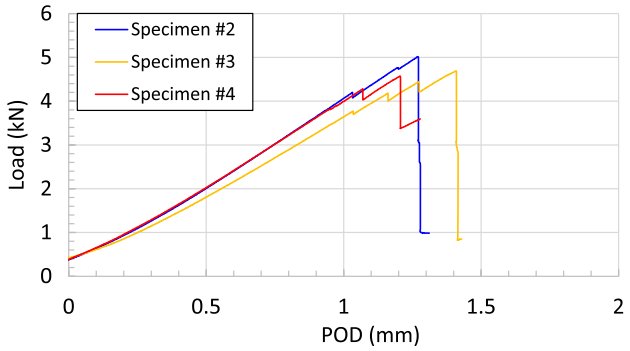

Fig. 2. Load-displacement curves from the three tests done at the University of Bristol. (For interpretation of the references to colour in this figure legend, the reader is referred to the web version of this article.)

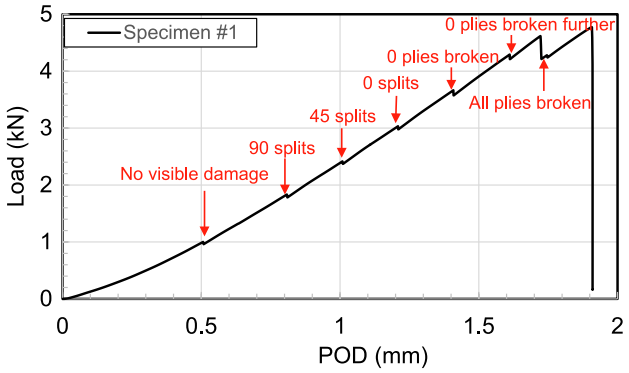

Fig. 3. Test result and damage information from *in situ* CT scans done at JAXA. (For interpretation of the references to colour in this figure legend, the reader is referred to the web version of this article.)

specimens [14]. The fracture process zones were examined at 95% of the average failure load for each size with different in-plane dimensions. However, it was not possible to determine how the fracture process zone grows at increasing load levels in the same specimen. This was only later simulated using a detailed finite element analysis of the scaled centre-notch configurations, but was limited to the growth of splits without considering fibre failure [15].

In this study a comprehensive experimental examination of the entire fracture process zone development has been conducted throughout *trans*-laminar fracture initiation in quasi-isotropic carbon/epoxy laminates using *in situ* CT scanning. *Ex situ* CT examination with dye penetrant was also carried out to better illustrate the 0° splits and explain their important stress blunting effects. Different 0° split lengths in the same test configuration at similar loads were generated by testing under both ambient and hot wet conditions. It was found that sub-critical damage occurred early in the tests, and the 0° splits delayed fibre breakage. Under hot wet conditions the 0° splits were longer due to the reduced intralaminar fracture toughness, further delaying fibre fracture.

2. Experimental set-up

Eccentrically loaded Single-edge-notch Tension (ESET) specimens were manufactured in accordance with the ASTM E1922 standard method for the characterisation of the *trans*-laminar fracture toughness of laminated polymer composites [13]. Fig. 1a shows the dimensions of the ESET specimens used. The material was HexPly® (Hexcel Corporation, USA) IM7/8552 unidirectional carbon/epoxy prepreg with two quasi-isotropic layups ($[45/90/\text{-}45/0]_{4s}$ and $[90/45/0/-45]_{4s}$), and a

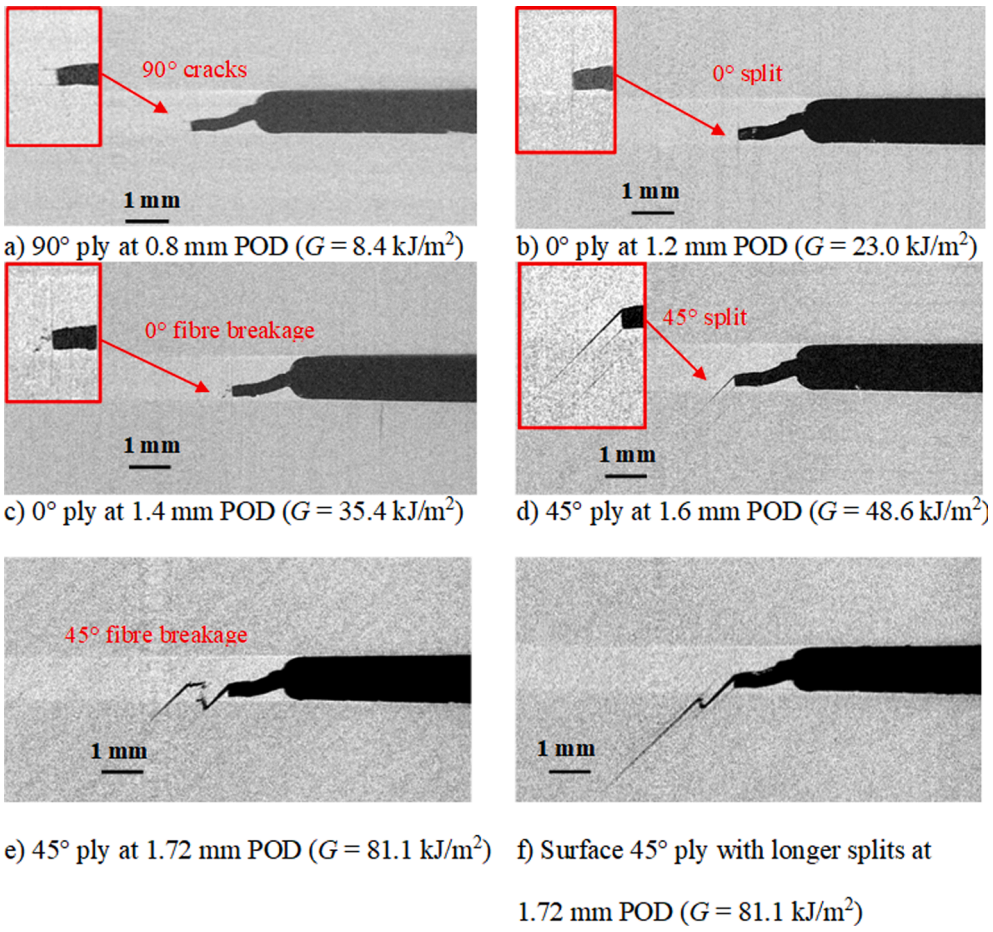

Fig. 4. Typical *in situ* CT scan images of different plies, taken from Specimen No. 1 at variable PODs (strain energy release rates). (For interpretation of the references to colour in this figure legend, the reader is referred to the web version of this article.)

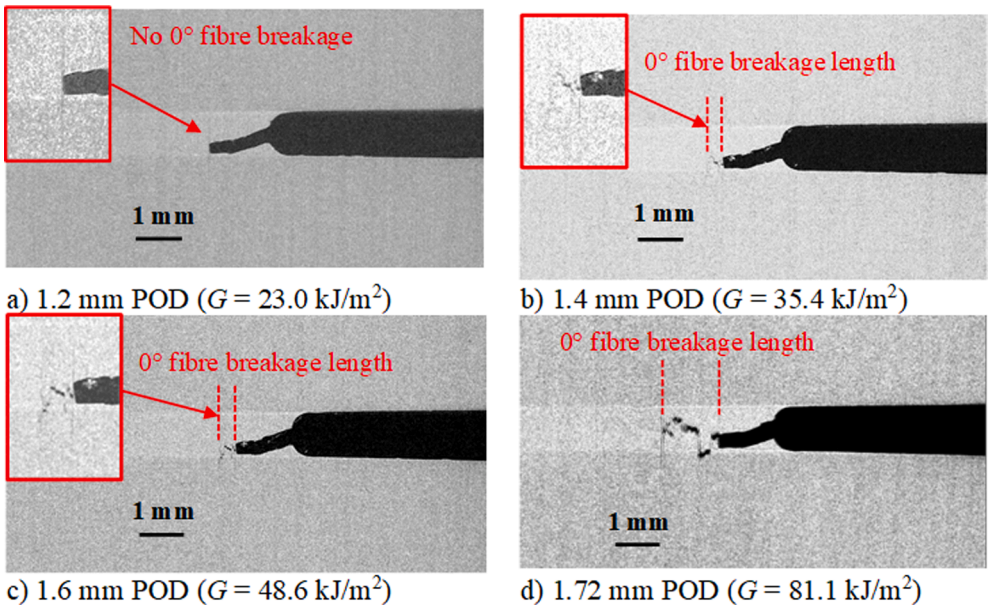

Fig. 5. Typical *in situ* CT scan images of 0° plies, taken from Specimen No. 1 at variable PODs (strain energy release rates). (For interpretation of the references to colour in this figure legend, the reader is referred to the web version of this article.)

nominal ply thickness of 0.125 mm and laminate thickness of 4 mm. The specimens, including the notches and holes, were cut from a plate using 1 mm carbide end mills on a Computer Numerical Controlled (CNC) router. The tips of the notches were extended manually by using a precise saw blade with a width of 0.25 mm. No cutting damage was visible at the holes.

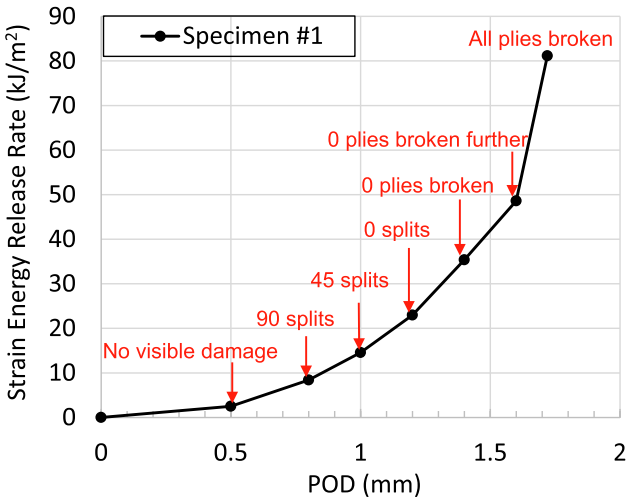

Fig. 6. Strain energy release rate curve and damage information from *in situ* CT scans. (For interpretation of the references to colour in this figure legend, the reader is referred to the web version of this article.)

The ESET specimens were attached to a test jig before loading, as shown in Fig. 1b. The test jig was then installed inside a polymer tube and was brought closer to the radiation source during CT scanning, as shown in Fig. 1c. The *in situ* CT scanner used was a Shimazu inspeXio SMX-225CT FPD HR scanner, with a 5 kN load cell installed. The voltage used was 200 kV and the electric current used was 120 μA. The number of projections per scan was 2400 and the exposure time was 250 ms. The angle swept was 360°. The voxel size was 10 μm. The customized *in situ* test rig was initially designed at the University of Bristol and then modified and manufactured at Japan Aerospace Exploration Agency (JAXA). During the initial linear loading phase, the tests at JAXA were paused at regular intervals, and the displacements were kept still. During each pause an *in situ* CT scan was carried out for about 30 minutes. After the initial linear loading phase, further scans were carried out after significant load drops.

Four ESET $[90/45/0/-45]_{4s}$ specimens were tested under displacement control. Specimens No. 1 was used for *in situ* CT scanning at JAXA. Specimens No. 2, No. 3 and No. 4 were tested on a Shimadzu screw-driven test machine with a load cell of 10 kN at the University of Bristol. These specimens were tested under ambient conditions. An additional specimen No. 5 from a different batch with a slightly different quasi-isotropic stacking sequence of $[45/90/-45/0]_{4s}$, was hot wet conditioned and tested in an environmental chamber on a 250 kN Zwick test machine at Zhejiang University. It was shown that the $[45/90/-45/0]_{4s}$ and $[90/45/0/-45]_{4s}$ laminates made of the same IM7/8552 prepreg have a similar initial fracture response [9], so their fracture process zones can be compared. Specimens No. 2 and No. 3 were tested up to failure. Specimens No. 4 and No. 5 were interrupted after the peak loads for *ex situ* CT scanning. They were soaked in a bath of zinc iodide penetrant for at least 3 days. The CT scanner used for *ex situ* examination was a Nikon XTH 225ST CT scanner. The voltage used was 102 kV and the electric current used was 208 μA. The number of projections per scan was 2000 and the exposure time was 500 ms. The angle swept was 360°. The voxel size was 19 μm.

3. Test results

Fig. 2 shows the load vs. Pin Opening Displacement (POD) graphs for Specimens No. 2, No. 3 and No. 4. All curves are shifted so the slopes for the linear parts go through the origin. The initial non-linear parts of the original curves are because of some compliance in the test jig. Then the curves are approximately linear up to the first load drop. Several small incremental load drops were present before the catastrophic failure. The catastrophic failure occurred after the peak load, and was caused by the compressive failure of the rear end of the specimen. These test results show that the overall response is similar, in terms of load drops. Specimen No. 4 was interrupted at 4.6 kN, and then prepared for *ex situ* CT scanning with dye penetrant.

Fig. 3 shows the load vs. POD curve from Specimen No. 1 and damage states at the pauses at which *in situ* CT scans were done at JAXA. The load drops slightly during the *in situ* CT scan, but it is considered small enough not to affect the results. The measured displacements are slightly different from the crosshead displacements shown in Fig. 2 due to different test set-ups, but they are not used for the calculation of strain energy release rates.

At Zhejiang University, Specimen No. 5 was conditioned at 80° Celsius and 85% relative humidity until four consecutive measurements showing no weight gain. It was tested at 120° Celsius up to 5.3 kN. Specimen No. 5 was then sent to the University of Bristol for *ex situ* CT scanning with dye penetrant, together with Specimen No. 4.

4. Results analysis

From every scan, a set of CT scan images through the specimen thickness were obtained. The colours of the CT scan images were flipped to make damage more obvious. There was a slight X-ray CT artifact due to the existence of the edge notch, but this did not affect the interpretation of damage. Fig. 4 shows the typical *in situ* CT scan images at different PODs. The other corresponding plies show similar damage patterns except for the surface 45° plies with longer splits. Based on these images, the damage states in the specimens were documented and labelled at the paused locations in Fig. 3. Specifically, no damage was observed at 0.5 mm POD. Then 90° ply cracks started to show at 0.8 mm POD (Fig. 4a). Between 1.0 and 1.2 mm POD, other splits including those in the 0° plies began to show (Fig. 4b). From 1.4 to 1.6 mm POD, the 0° plies were seen to be broken (Fig. 4c) but not the 45° plies (Fig. 4d). No obvious load drops were observed, except for those first six slight artificial load drops up to 1.6 mm POD in Fig. 3 due to CT scanning pauses. The 45° plies were only seen to be broken at 1.72 mm POD

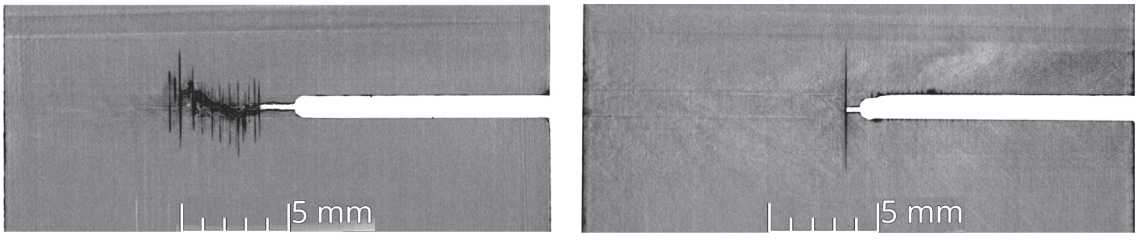

a) Room temperature dry Specimen No. 4 interrupted at 4.6 kN

b) Hot temperature wet Specimen No. 5 interrupted at 5.3 kN

Fig. 7. Comparison of initial splits in *ex situ* CT scan images of two typical single 0° plies with dye penetrant under different environmental conditions.

(Fig. 4e), which marks the full breakage through the specimen thickness. Finally, compressive failure occurred at the rear of the specimen at about 1.9 mm POD, which is the end of the test. Delamination could not be clearly observed without dye penetrant, which could not be used in these *in situ* tests. Splitting may also be under-estimated without dye penetrant.

The *in situ* CT scans help better understand the damage development, and also yield objective crack increments. As discussed by Xu et al. [16], the crack length can be defined in different ways. Here, an effective crack length, a, based on the average fibre breakage length in the broken 0° plies, Δa, plus the machined notch length, a_0, was used for the calculation of stress intensity factors. Specifically, the crack increment in each ply, Δa, was measured from the *in situ* CT scan images (typical ones illustrated in Fig. 5) by using VG Studios Max (Volume Graphics, Germany) and Dragonfly (Object Research Systems, Canada). It was added to the initial machined notch length, a_0, for each pause location in Fig. 3. The stress intensity factor, K, can then be calculated based on the equation in ASTM E1922 [13] and the measured effective crack lengths:

$$K = \frac{P}{B\sqrt{W}}\alpha^{\frac{1}{2}}(1.4+\alpha)[3.97 - 10.88\alpha + 26.25\alpha^2 - 38.9\alpha^3 + 30.15\alpha^4 - 9.27\alpha^5]/(1-\alpha)^{\frac{3}{2}} \quad (1)$$

where P is the interrupted load or the load drop (e.g. 3.0 kN for 1.2 mm POD, 3.7 kN for 1.4 mm POD, 4.3 kN for 1.6 mm POD and 4.6 kN for 1.72 mm POD); $a = a_0 + \Delta a$ is the effective crack length; $\alpha = a/W$; B is the specimen thickness; W is the specimen width.

The specimen thickness is relatively small compared to the specimen width at 16%, so it is reasonable to assume plane stress. Therefore, stress intensity factor can be converted to strain energy release rate, G:

$$G = \frac{K^2}{E} \quad (2)$$

where E is Young's modulus of the current quasi-isotropic laminate, which was reported to be 61.6 GPa [15].

The strain energy release rate at each pause location is determined and thus the relationship between the strain energy release rate and damage evolution can be established. In Fig. 6, the pause locations are spread across the whole displacement range, so damage zone development up to the point of propagation can be studied. Sub-critical damage such as 90° ply cracks initiated early on from as low as 8.4 kJ/m^2 (Fig. 4a). Many 0° plies were seen broken at 48.6 kJ/m^2 (Fig. 5c). But all plies were only broken at 81.1 kJ/m^2 (Fig. 5d) which can be defined as the critical strain energy release rate or fracture energy for propagation. The critical value is within 5% of the reported fracture energy value of 85 kJ/m^2 [17] at initial fracture propagation based on the same method for effective crack measurement in the 0° plies from over-height compact tension specimens with the same material and layup.

Specimen No. 4 was compared against Specimen No. 5 made of the same material but of a slightly different quasi-isotropic stacking sequence and tested under hot wet conditions. Both were interrupted at the labelled loads and treated with dye penetrant afterwards. The splits, at the notch tip can be examined by *ex situ* CT scanning, as shown in Fig. 7. It is known that hydrothermal ageing reduces the shear strength and interlaminar fracture toughness of the matrix [18], so the initial 0° splits were able to grow longer under hot wet conditions (Fig. 7b). The longer initial 0° splits blunted the stress concentration at the notch tip, and therefore delayed any fibre breakage up to a load at least 15% higher than the peak load under ambient conditions. Because hydrothermal aging is not expected to affect the properties of the fibres, this particularly demonstrates the significant role of 0° splits during *trans*-laminar fracture initiation. Delamination was observed in Specimen No. 4 at room temperature dry condition and in Specimen No. 5 at hot temperature wet condition, but the dominant features were splitting and fibre breakage in the 0° plies.

5. Discussion

No dye penetrant was applied to the specimens when *in situ* CT scanning was performed. It is plausible that some splitting and delamination were not detected. Therefore, dye penetrant was used in the extra *ex situ* CT scans from which the split lengths were quantitively compared at different environmental conditions. In addition, accurate strain energy release rate calculations rely on the knowledge of crack increments in the 0° plies, and these crack increments were very clear under loading during *in situ* CT scanning even without dye penetrant.

The current ESET specimens were found to be too small to derive a full R-curve [12] so the focus of the current work has been about translaminar fracture initiation. The main limitation of the current specimen geometry is its small ligament width. As the crack grows longer, the FPZ is no longer small-scale compared to the remaining ligament and compressive failure at the rear end can also occur, so the derived R-curves are not reliable.

6. Conclusions

The current work made use of *in situ* and *ex situ* CT scanning for the experimental examination of the fracture process zone development in quasi-isotropic carbon/epoxy laminates. With *in situ* CT scanning, the detailed damage sequence was examined, and accurate crack increments were measured continuously in a single specimen. Using these crack increments based on the average fibre breakage length in the 0° plies, the strain energy release rate value for each damage state was calculated in accordance with the ASTM E1922 standard [13] throughout the entire fracture process zone development.

It was observed that the sub-critical damage such as 90°, 45° and 0° splits started to appear from an early stage in the tests, followed by 0° fibre breakage and then all plies were broken. Longer initial 0° splits were seen under hot wet than ambient conditions, which delayed any fibre failure until a higher load. These results provide direct confirmation of the key role that the 0° splits play during fracture process zone development.

In addition to the newly observed damage process zone development, the *in situ* obtained fracture energy when all plies are broken was also compared against the previously reported value for initial fracture propagation derived from *ex situ* CT scans on specimens with a different geometry [17]. A good agreement was achieved based on the same definition of crack length, confirming the reliability of the current method.

CRediT authorship contribution statement

Xiaodong Xu: Conceptualization, Methodology, Validation, Investigation, Formal analysis, Resources, Data curation, Writing – original draft, Project administration, Funding acquisition. **Shin-ichi Takeda:** Investigation, Data curation. **Michael R. Wisnom:** Writing – review & editing.

Declaration of Competing Interest

The authors declare that they have no known competing financial interests or personal relationships that could have appeared to influence the work reported in this paper.

Data availability

The raw/processed data required to reproduce these findings cannot be shared at this time as the data also forms part of an ongoing study.

Acknowledgements

The author would like to thank Dr Bowen Gong for conditioning and

testing the specimen at Zhejiang University. The author would also like to thank Dr Andre Jesus from Loughborough University for feedback on the manuscript.

References

[1] Pinho ST, Robinson P, Iannucci L. Fracture toughness of the tensile and compressive fibre failure modes in laminated composites. Compos Sci Technol 2006;66(13):2069–79.
[2] Zobeiry N, Vaziri R, Poursartip A. Characterization of strain-softening behavior and failure mechanisms of composites under tension and compression. Compos A Appl Sci Manuf 2015;68:29–41.
[3] Catalanotti G, Camanho PP, Xavier J, Dávila CG, Marques AT. Measurement of resistance curves in the longitudinal failure of composites using digital image correlation. Compos Sci Technol 2010;70(13):1986–93.
[4] Bergan A, Dávila C, Leone F, Awerbuch J, Tan T-M. A Mode I cohesive law characterization procedure for through-the-thickness crack propagation in composite laminates. Compos B Eng 2016;94:338–49.
[5] Catalanotti G, Arteiro A, Hayati M, Camanho pp.. Determination of the mode I crack resistance curve of polymer composites using the size-effect law. Eng Fract Mech 2013;118:49–65.
[6] Maimí P, Ortega A, González EV, Costa J. Should the translaminar fracture toughness of laminated composites be represented by the R or the J curve? A comparison of their consistency and predictive capability. Compos A Appl Sci Manuf 2022;156:106867.
[7] Garcea SC, Wang Y, Withers PJ. X-ray computed tomography of polymer composites. Compos Sci Technol 2018;156:305–19.
[8] Xu X, Wisnom MR, Mahadik Y, Hallett SR. Scaling of fracture response in over-height compact tension tests. Compos A Appl Sci Manuf 2015;69:40–8.
[9] Xu X, Sun X, Wisnom MR. Initial R-curves for trans-laminar fracture of quasi-isotropic carbon/epoxy laminates from specimens with increasing size. Compos Sci Technol 2021;216:109077.
[10] Rev T, Nachman T, Kap I, Shor O, Shemesh N, Mollenhauer D, et al. Architecture effects for mode I trans-laminar fracture in over-height compact tension tests: damage propagation and fracture response. Compos A Appl Sci Manuf 2022;159:106987.
[11] Buffiere JY, Maire E, Adrien J, Masse JP, Boller E. In situ experiments with X ray tomography: an attractive tool for experimental mechanics. Exp Mech 2010;50(3):289–305.
[12] Sun X, Takeda S, Wisnom MR, Xu X. In situ characterization of trans-laminar fracture toughness using X-ray computed tomography. composites. Communications 2020;21:100408.
[13] ASTM, Standard, E1922–97.. Standard test method for translaminar fracture toughness of laminated polymer matrix composite materials. West Conshohocken, PA, USA: ASTM International; 1997.
[14] Xu X, Wisnom MR, Mahadik Y, Hallett SR. An experimental investigation into size effects in quasi-isotropic carbon/epoxy laminates with sharp and blunt notches. Compos Sci Technol 2014;100:220–7.
[15] Xu X, Wisnom MR, Li X, Hallett SR. A numerical investigation into size effects in centre-notched quasi-isotropic carbon/epoxy laminates. Compos Sci Technol 2015;111:32–9.
[16] Xu X, Wisnom MR, Hallett SR. Deducing the R-curve for trans-laminar fracture from a virtual Over-height Compact Tension (OCT) test. Compos A Appl Sci Manuf 2019;118:162–70.
[17] Xu X, Takeda S, Aoki Y, Hallett SR, Wisnom MR. Predicting notched tensile strength of full-scale composite structures from small coupons using fracture mechanics. Compos Struct 2017;180:386–94.
[18] Yu B, Katafiasz TJ, Nguyen S, Allegri G, Finlayson J, Greenhalgh ES, et al. Hygrothermal effects on the translaminar fracture toughness of a highly toughened aerospace CFRP: experimental characterisation and model prediction. Compos A Appl Sci Manuf 2021;150:106582.